

Localized flow control in microchannels using induced-charge electroosmosis near conductive obstacles

K. V. Sharp · S. H. Yazdi · S. M. Davison

Received: 7 July 2010 / Accepted: 13 December 2010 / Published online: 29 December 2010
© Springer-Verlag 2010

Abstract In this paper, we investigate the use of induced-charge electroosmosis (ICEO) as a means of providing localized flow control near conductive obstacles within bulk pressure-driven flow. In an experimental device, this ICEO flow was induced by an on/off switchable AC field applied across a section containing gold post(s). A simple numerical model, adapted from Levitan et al. (Colloids Surf A 267:122–132, 2005), was implemented and used to provide guidance for the design of the experimental devices. The induced flow was combined with an applied bulk pressure-driven flow to modify flow patterns. We have specifically observed single and multiple stream patterns downstream of the posts in the experimental devices, suggesting the presence of ICEO flow in the experimental system. The custom devices were obtained using a fabrication process that relies on relatively standard steps in the MEMS community, however, unlike other fabrication processes, it has been shown to create fully conductive posts with vertical sidewalls. Utilizing various combinations of number(s) of post(s), geometry and position, useful flow patterns can be created.

Keywords Microfluidics · Induced-charge electrokinetics · Conductive posts · Particle manipulation

1 Introduction

Microfluidics has been an area of abundant research and rapid advancement in the last few years. A wide range of applications from sensor technology (Springer et al. 2010) to lab-on-a chip systems (Novak et al. 2007) have benefited from this research. The breadth of the advancements in microfluidics has been reviewed in recent texts (Squires and Quake 2005; Whitesides 2006). One key use of microfluidics garnering attention is the manipulation of particles. In some cases, particle manipulation may be valuable in helping to identify the type or condition of biological cells (Liu et al. 2006), analyze the health of cells (Komen et al. 2008), or observe effects of drug treatments (Liu et al. 2007). In other cases, manipulation of particles for the creation of biomaterials (Hung and Lee 2007) or the manufacture of novel surfaces through patterning (Cong et al. 2010) in a microfluidic system is useful.

Thus, a key capability for microfluidic-based systems is the ability to manipulate suspended particles, directing them toward or away from regions within the device, particularly for detection applications. Some methods such as hydrodynamic focusing (Mao et al. 2007), microvortex manipulation (Hsu et al. 2008), or entropic separations (Dinsmore et al. 1996) are effective in simple focusing of particles. These methods rely on fixed channel characteristics or flow conditions that limit their flexibility and consequently the range of particles or applications in which the focusing is effective. External forces can be used to aid in particle manipulation including those generated by magnetic fields (Desai et al. 2007), acoustics (Shi et al. 2008), electric fields (Zhang et al. 2010; Demierre et al. 2007), or optics (Chiu et al. 2005; Appleyard and Lang 2007). A controllable external force can lead to a greater range of focusing functions, and can also allow intermittent application.

K. V. Sharp (✉)
Mechanical, Industrial, and Manufacturing Engineering,
Oregon State University, Corvallis, OR 97331, USA
e-mail: kendra.sharp@oregonstate.edu

S. H. Yazdi · S. M. Davison
Department of Mechanical and Nuclear Engineering, The
Pennsylvania State University, University Park, PA 16802, USA

In this article, induced-charge electroosmosis (ICEO) is presented as a means of flow manipulation which results in manipulating the suspended particles in the fluid. ICEO is aptly named because the fluid motion is caused by the action of the electric field on the induced electrical double layer (EDL) surrounding a polarizable object. The phenomenon was originally termed ICEO by Squires and Bazant (2004, 2006) and is the generalization to any polarizable surface of “AC electroosmosis” which was observed at electrode surfaces in AC electric fields (Ramos et al. 1998, 1999; Ajdari 2000). Similar flows around metallic colloids with fixed total charge have been shown in the Russian literature (Gamayunov et al. 1986; Murtsovkin 1996). A very recent review of induced-charge electrokinetic phenomena has been published by Daghighi and Li (2010). Typically, the application of ICEO results in recirculation regions surrounding a polarizable object. ICEO and the resulting flow fields have been proposed as a means of manipulating fluid flows in a corner, selecting flows in a T-junction, or as a means of fluid mixing (Harnett et al. 2008). The majority of publications on ICEO flow are either theoretical (Bazant et al. 2004, 2009a, b; Zhao and Yang 2009) or numerical (Jain et al. 2009; Sugioka 2010). The first experimental observation of this phenomenon around a metal wire was carried out by Levitan et al. (2005). To date, there is limited experimental evidence on ICEO flow (Eckstein et al. 2009; Pascall and Squires 2010) especially near polarizable posts. Previous experimental work has mainly focused on mixing applications (Harnett et al. 2008).

In the present work, ICEO is applied as a means of locally manipulating the flow and particles suspended therein in a microdevice for a specific purpose, such as concentrating particles in desired regions of the channel. Multiple fixed conducting objects are precisely positioned in the microchannel so that the on/off switchable ICEO flow field can be combined with a background pressure flow to enable flow manipulation. Flexibility is a key component of this strategy, as the design of the conducting objects can be changed to produce devices with different levels of manipulation or different functions. Also, the presence of the ICEO flow can be switched on and off rapidly because of its dependence on an applied AC electric field providing highly controllable, intermittent manipulation. In order to provide this flexibility in design, a novel and simple fabrication technique was developed. Note that Harnett et al. (2008), in supplementary documents accompanying their article, have described two promising fabrication techniques, though these techniques have the disadvantage of not being able to create vertical sidewalls of the conducting objects.

2 Theoretical background

To illustrate ICEO fluid flow, consider the case of an electrically isolated, fixed metallic post in a fluid-filled microchannel. When an electric field is applied across the metallic post, the electrons within the post rearrange so that it is polarized. The accumulation of charges at the ends of the post attract oppositely charged ions in the surrounding fluid, which accumulate at the ends forming induced electrical double layers of opposite charges. The electric field acts on the induced EDL according to the same principles as DC electroosmosis, in that the ions in the diffuse part of the EDL move toward the oppositely charged electrode. However, in ICEO, the charges that are moving at each end of the post are doing so in opposite directions creating a flow pattern where the flow is directed toward the ends of the post and away from the post at its equator. The steady flow field that develops around an isolated post is a quadrupole arrangement of recirculation regions (Squires and Bazant 2004). An example of flow field around an isolated post is shown in Fig. 1a.

When the electric field is reversed, in the case of an applied AC signal, the polarization and consequently the EDLs that are induced will be oppositely charged. However, since the electric field is also reversed, the ICEO flow pattern remains unchanged. In an AC electric field, the ICEO flow does not have to compete with standard DC electrokinetic motions, so long as the frequency of the AC field is selected such that the DC motion of the ions under one polarity for half a cycle is small. Recall that when the polarity is switched in the other half of the cycle, the flow due to the AC field remains unchanged, but the DC motion under the opposite polarity is in the opposite direction. Flexibility in flow patterns is achieved by combining localized AC-induced ICEO flow with a bulk background flow.

The mathematical model of the ICEO flow in Fig. 1a follows that presented in Levitan et al. (2005) and is briefly summarized here. The assumption of thin electrical double layers simplifies the system, and is physically reasonable within the current experimental system. Thus, the EDL is modeled as electrical potential in the bulk outside the EDL, ϕ ,

$$\nabla^2 \phi = 0. \quad (1)$$

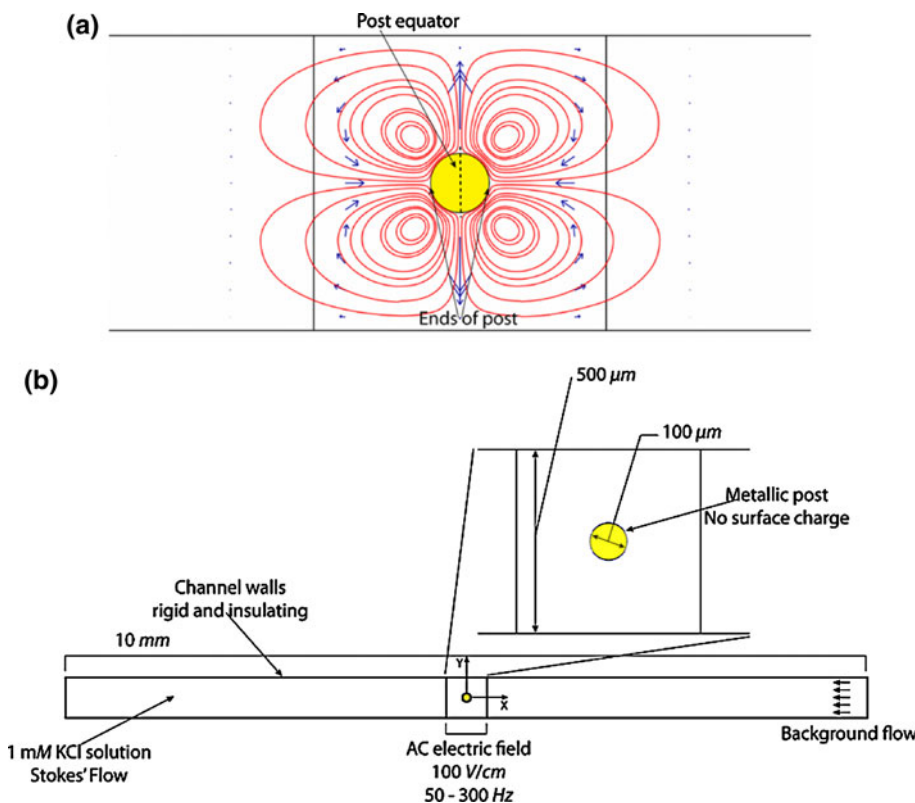
The channel walls are non-polarizable and insulating so the boundary condition is zero normal current,

$$\mathbf{n} \cdot \nabla \phi = 0, \quad (2)$$

where \mathbf{n} is the unit normal to the surface. The capacitive model of the EDL on the polarizable surface consists of two capacitors in series, a linear surface capacitor, C_S , based on Stern’s model of the EDL and then a diffuse-layer

Fig. 1 a Fluid streamlines demonstrating the quadrupole arrangement of recirculation constituting ICEO flow around a conducting post under the action of an AC electric field.

b Schematic (top view) of a 2D slice out of the microfluidic channel used for ICEO flow. Relevant dimensions and system parameters indicated



capacitor, C_D , from Gouy’s EDL model (Levitan et al. 2005). The effect of each capacitor is controlled by the ratio, $\delta = C_D/C_S$, which allows altering the model of the EDL from a diffuse Gouy–Chapman model to a surface Helmholtz model. This parameter, δ , can also serve as a fitting parameter for matching the numerical models to experimental data (Levitan et al. 2005), though we did not expressly use it to “fit” the present experimental data and numerical models (see the discussion in Sect. 3.1). More complicated, nonlinear models for the induced EDLs exist, and can provide improved accuracy but are significantly more computationally intensive (Soni et al. 2007). Since the numerical models described herein were used primarily to motivate and predict flows in actual devices, the simpler and more efficient model suggested by Levitan et al. (2005) provides the basis for the numerical work outlined here.

The surface electrical boundary condition relates the bulk current to the capacitive charging of the EDL,

$$\sigma \mathbf{n} \cdot \nabla \phi = C_D \frac{d\zeta}{dt}. \tag{3}$$

The bulk conductivity, $\sigma = \varepsilon D/\lambda^2$, is determined by the permittivity of the solution, ε , diffusion constant, D , and the EDL thickness, λ . The diffuse-layer capacitance is the ratio of the permittivity to the EDL thickness, $C_D = \varepsilon/\lambda$. The final component of the boundary condition is the zeta potential, ζ , which unlike the DC case, is induced by the

applied field and varies in space and time. The value of the induced zeta potential, on the surface of the conducting post, is determined by the voltage across the EDL,

$$\zeta = \frac{\phi_0 - \phi}{1 + \delta}, \tag{4}$$

where ϕ is the potential in the bulk at the boundary with the EDL and ϕ_0 is the potential of the wire (Levitan et al. 2005). In this case, the plain metallic wire is assumed to have no native charge, it is not connected to any potential, and located at the center of the applied AC field so $\phi_0 = 0$.

Similarly, the fluid mechanics problem reduces to a matter of determining the impact of the induced flow at the surface on the bulk motion. The thin EDL approximation confines the induced electrokinetic motion to the EDL which then serves as a boundary condition to the bulk flow. Due to the low Reynolds number, Stokes’ equations govern the bulk fluid motion, \mathbf{u} ,

$$\nabla \cdot \mathbf{u} = 0, \tag{5}$$

$$\eta \nabla^2 \mathbf{u} = \nabla p, \tag{6}$$

where η is the fluid viscosity and p is the pressure field. The tangential velocity boundary condition on the conducting post is the same as for DC electrokinetics,

$$\mathbf{u}_{\parallel} = \frac{\varepsilon \zeta}{\eta} \nabla_{\parallel} \phi, \tag{7}$$

which defines the tangential fluid velocity, $u_{||}$, at the surface given the fluid properties, zeta potential, and electric field. As opposed to DC electrokinetics, in ICEO flow the zeta potential is induced by and is a function of the applied electric field, creating a boundary condition that is second order in electrical potential, ϕ .

The ICEO flows under investigation are induced by an AC electric field and thus the flow fields that develop vary with time. The desired frequency of the AC electric field is determined by examining the charging time of the EDLs in the system. The charging time can be determined by properties of the system: $\tau = \lambda a/D$, where a is the diameter of the conducting post. For the system under investigation, a charging time of $\tau = 0.5$ ms is estimated. This charging time corresponds to a frequency of $\omega = (2\pi\tau)^{-1} = 318$ Hz. Applying an AC electric field with a frequency up to this value yields the ICEO flow, as the EDLs have time to become fully charged resulting in the highest induced zeta potential. It is also possible to institute a lower limit to the applied frequency. Since ICEO effects can be of a reduced magnitude compared to DC electrokinetic motions, it is preferable to apply a frequency that minimizes standard DC electrokinetic motions. In the physical system addressed here, DC motions are suppressed with an AC electric field of the order of 50 Hz.

3 Numerical work

3.1 Numerical model

The primary use of a numerical model in this article is to explore the effect of various geometries and placements of posts for the experimental device design. The basic microfluidic system under investigation, both numerically and experimentally, is presented schematically in Fig. 1b. This represents a 2D slice out of the center of the microfluidic channel so that the computational load is reduced. The conducting post is located in the center of the channel. The two vertical lines near the post represent the electrodes that supply the AC electric field. A pressure difference between the inlet and outlet creates a bulk background flow in the system. The walls of the channel are assumed to be insulating and to carry a uniform negative zeta potential. The basic design of the device is for bulk fluid motion in the channel to move past a region of ICEO flow that acts on particles suspended in the bulk fluid. The number and positioning of the conducting posts in the channel determine the overall ICEO flow pattern, while the strength of the AC electric field determines the magnitude of the focusing effect. The primary goal of the numerical investigation was

to identify potential arrangements of posts for use in the experimental devices.

The system of equations has been successfully implemented to solve for time-averaged ICEO flow using a commercial finite-element package, Comsol Multiphysics (Comsol AB, Burlington, MA). Application of an AC electric field creates a model that varies in time. The model is set to run through at least 11 periods of the applied AC electric field, with a minimum of seven velocity samples recorded per model period to eliminate aliasing. The mesh has a high density in the region of the conducting posts and expands to a lower density in the regions of the channel with uniform background flow (Davison 2009).

The specific values of the physical properties used in the numerical model are given in Table 1. Prior to fabrication, the values not specific to a particular post design (e.g. δ and C_D) were selected to match the most relevant previous experimental data of Levitan et al. (2005). Since the present experimental conditions were similar to those of Levitan et al. (2005), the assumption was made that the structure of the EDL would also be similar, and δ was held constant for the remainder of the computations. The values of physical parameters such as viscosity, permittivity, and so forth, were adjusted to represent the experimental conditions at the time of data collection.

3.2 Numerical results

The time-averaged flow field for a microchannel with one post is shown in Fig. 2a. Bulk pressure-driven flow seen in most of the channel demonstrates that AC electric field does not affect the bulk flow in the system. The localized effect, therefore, opens the possibility of integrating ICEO sections into existing microfluidic devices without interruption of the existing flow characteristics.

Table 1 Numerical simulation parameters

Parameter	Definition	Value
ε	Bulk permittivity	7.08×10^{-10} F/m
η	Viscosity	1×10^{-3} Pa s
σ	Bulk conductivity	0.014 S/m
C_D	Diffuse-layer conductance	0.071 C/V
δ	Capacitance ratio	18
ϕ_{ICEO}	Applied AC potential	1 V
ω	Applied frequency	300 Hz
D	Diffusivity	2×10^{-9} m ² /s
λ	EDL thickness	10 nm
a	Diameter of conducting post	100 μ m
Re	Ratio of inertial to viscous fluid forces	1×10^{-3}

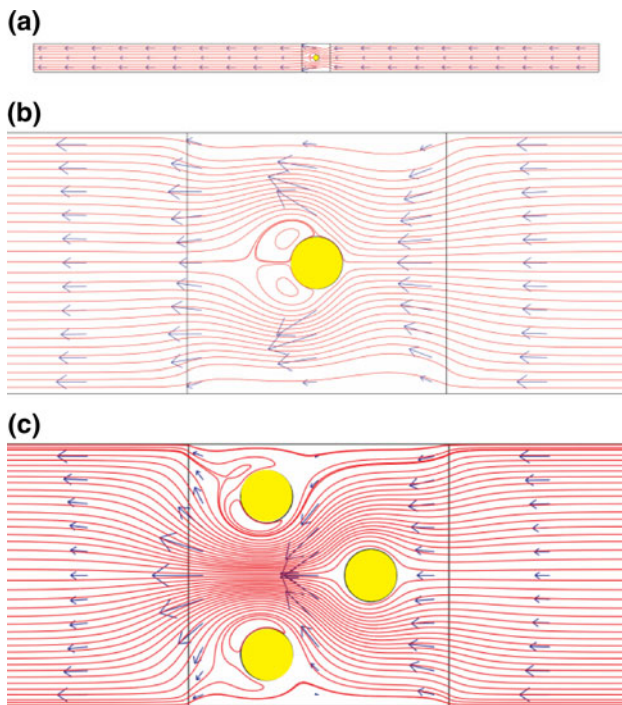


Fig. 2 ICEO flow in a microfluidic channel. **a** Streamlines detailing the fluid motion throughout the entire channel, demonstrating the ICEO flow region around the post, **b** fluid streamlines in the vicinity of the conducting post demonstrating the combination of ICEO flow and a pressure-driven background bulk flow, **c** a combination of conducting posts with interacting ICEO flows can create a flow field useful for particle and fluid manipulation

The details of the ICEO region around a single post are shown in Fig. 2b. The quadrupole pattern seen in the quiescent system is reduced to two recirculation regions on the trailing side of the post. The leading recirculation regions are largely acting in the direction of the oncoming bulk flow and so are absent. Potentially, more interesting flow fields can be created with additional posts in the flow. Figure 2c contains the average flow field around a series of three conducting posts. With multiple posts in close proximity, the ICEO flows that develop interact with those of other posts. The combined flow field indicated here illustrates a potential flow-focusing scenario. The incoming streamlines, from throughout the upstream channel, pass around the leading post and are compressed to pass between the remaining posts.

4 Experimental work

4.1 Device fabrication

A microchannel device containing conductive posts was fabricated in order to demonstrate the use of on/off switchable localized flow control. Typical lithographic

processes were employed since they enable a high level of control of the size and placement of the posts, both of which are critical to device functionality.

A silicon wafer served as the base for the process, upon which a photolithographic pattern of microchannels containing fluid wells was applied using photoresist (SPR 220). A typical channel was 2.5 mm long with a width of 500 μm . The desired pattern was etched into the silicon wafer to a depth of 10 μm by deep reactive ion etching (DRIE). A layer of silicon dioxide was coated on the surface of the wafer by thermal oxidation on the surface of the wafer to produce insulating channel walls for the device. A 50 nm layer of chrome metal (Cr) followed by a 100 nm layer of gold metal (Au) was sputtered over the oxide. Cr was used to promote Au adhesion to the oxide layer. This seed layer provides the necessary conductive layer on the outside of the wafer for electrochemical deposition. Another layer of photoresist is applied and patterned everywhere except in the target post region. Electrodeposition is then used to grow the gold posts with different diameters of 100, 200, and 300 μm at desired location(s). During electrodeposition, a profilometer is used frequently to ensure that the gold pillar structures do not exceed the desired height. After the deposition process, the remaining gold and chrome seed layer is removed using gold and chrome etchant solvents, respectively, leaving a silicon dioxide channel structure containing gold posts. The wafer containing the channels and conductive post is then capped by polydimethylsiloxane (PDMS). Access holes in the PDMS cap allow for the addition of fluid and electrodes to the wells. Utilizing this process, channels containing precisely sized and located conducting posts have been created. The process flow for fabrication is shown in Fig. 3a. An image of the fabricated channel containing three gold posts is shown in Fig. 3b. The fluid wells are located on either end of the channel and provide access for the fluid and application of the electrical field. Field emission scanning electron microscope (FESEM) pictures of a microchannel containing three and two posts are shown in Fig. 4a and b, respectively.

4.2 Experimental setup

The working fluid for the experiments was a 1 mM KCl solution (140 $\mu\text{S}/\text{cm}$). The fluid was seeded with 1 μm fluorescent polystyrene particles (Invitrogen Corp., Carlsbad, CA) to allow for visualization of the flow. The concentration of particles in the fluid was 0.02% by volume. A function generator created a 10 Vp-p sinusoidal signal that was passed through an amplifier with a gain of up to 100 \times to increase its magnitude. The AC field was applied across the microchannel through platinum wires inserted into the

Fig. 3 **a** Process flow diagram for the manufacture of a microfluidic channel containing gold posts. The gold posts are electrodeposited onto a silicon wafer through a photoresist mask. PDMS is used to cap the channels, **b** image of the completed channel containing three gold posts. The fluid wells are located on either end of the channel and provide access for the fluid and application of the electrical field

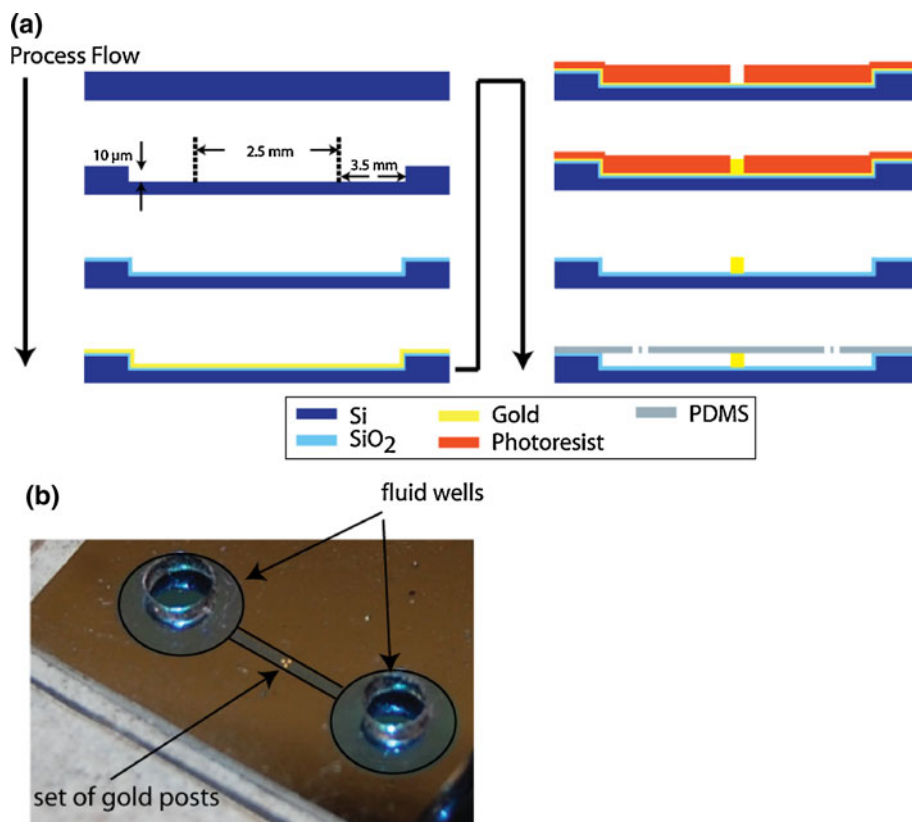
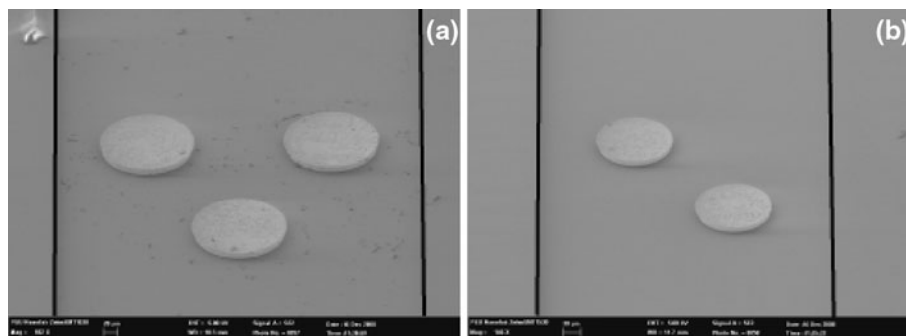


Fig. 4 FESEM images of the channels and the posts. **a** Image of a channel containing three posts, **b** image of a channel containing two posts



fluid wells. Since the ICEO flow is boundary-driven on the conducting post(s) and a function of the tangential electric field on the post, applying the potential difference in the wells is compatible with the numerical models so long as the tangential electric field at the post is consistent in the two cases. No electrolysis was observed on the surface of the posts under any of the included experimental conditions, nor under the condition of twice the magnitude of applied potential. A syringe pump was used to drive a low volume rate of fluid creating a bulk pressure-driven flow through the microchannel. A standard video microscopy system was used to record a series of images of the flow field for analysis, with an in-line TRITC bandpass filter for reduction of background noise (e.g. reflection from walls). The images were captured at 10 frames per second (fps),

where each image was 640×512 pixels, for 200–300 images. The magnification was limited both by optical access to the test section and the requirement that no portion of the flow loop could be disturbed during a test run.

4.3 Image analysis

The initial step in analysis was to remove the background from the captured images. This process was carried out to remove the image of any particle that had adhered to the post and the top or bottom surfaces. The pixel-by-pixel average image was computed for each series of captured images, which contained bright spots where particles adhered to the top or bottom surface.

$$I_{avg}(x, y) = \frac{1}{N} \sum_{n=1}^N I_n(x, y), \tag{8}$$

where N is the total number of frames. The intensity of moving particles in each frame, $I'_n(x, y)$, is equal to the intensity of the individual frame less the series average, $I_n(x, y) - I_{avg}(x, y)$.

$$I'_n(x, y) = I_n(x, y) - I_{avg}(x, y). \tag{9}$$

Particle pathlines are created by summing the individual moving particle intensities over all N frames in the series,

$$I'_{sum}(x, y) = \sum_{n=1}^N I'_n(x, y). \tag{10}$$

To assess the probability distribution of particles in the spanwise direction, the intensity of signal (due to moving particles), $I'_{norm}(x, y)$ (defined in Eq. 11), at a given streamwise position, y , is normalized by dividing $I'_{sum}(x, y)$ by the integral of $I'_{sum}(x, y)$ over the width of the channel (W).

$$I'_{norm}(x, y)|_{y=L} = \frac{I'_{sum}(x, y)}{\int_0^W I'_{sum}(x, y) dx} \Big|_{y=L}. \tag{11}$$

Note that the values of $I'_{norm}(x, y)$ depend on both the seeding density and the number of times a particle occurs at that specific location each time a frame is acquired; the values shown in Figs. 5 and 6 are best interpreted as a relative measure of probability of occurrence in the spanwise direction.

5 Results and discussion

The streamlines observed for flow around the posts confirmed the presence of ICEO flow in the near post region. A comparison of the streamlines and spanwise intensity profiles, $I'_{norm}(x, y)$, in the absence and presence of the AC electric field, is presented in Figs. 5 and 6. The images of streamlines without the AC field (Figs. 5a and 6a) are indicative of Stokes' flow around the post. When the AC field is applied, the ICEO flow that develops around the post is evidenced by the creation of a wake downstream of the post. However, the incoming flow upstream of the posts does not appear affected when the AC field was switched on and off, while changes were immediately noticeable in the "local" region near the posts, where the images were acquired. This wake devoid of particles is seen to persist for at least four to five post diameters; further observation is not possible due to the competing constraints for viewing the

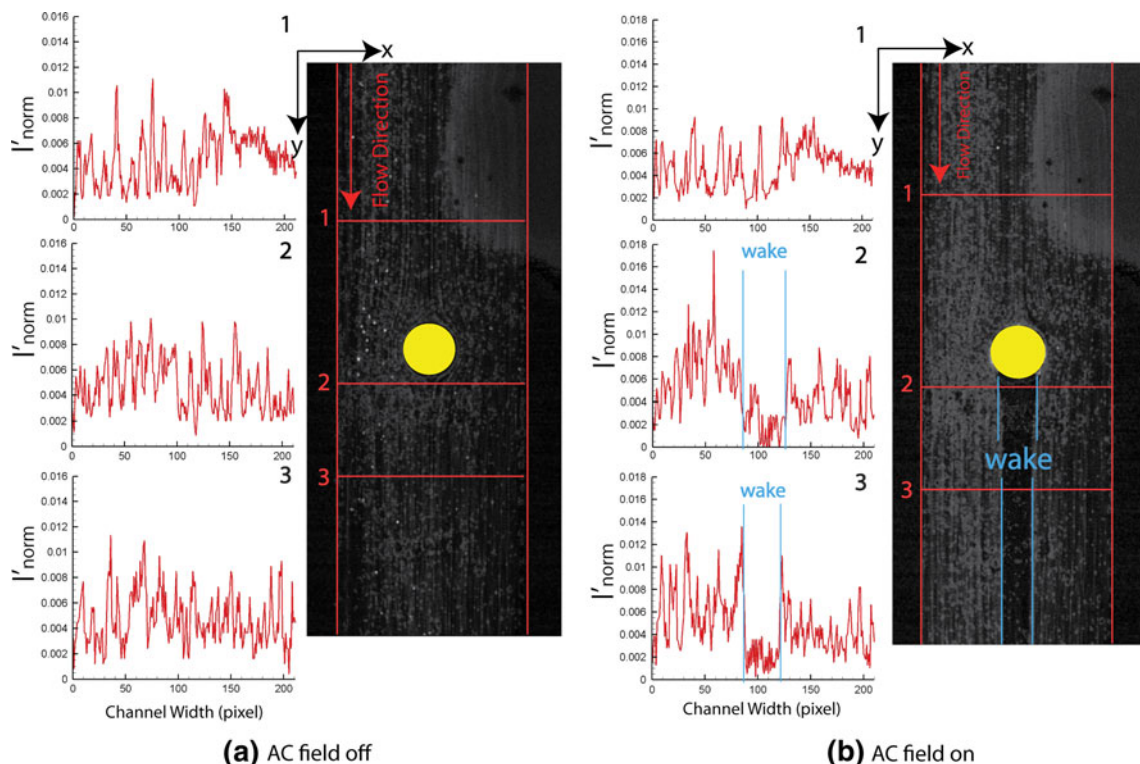


Fig. 5 Streamlines around a single circular post positioned in the center of the microchannel with a pressure-driven background flow: **a** AC field is off, **b** AC field is on, $V = 50$ Vp-p

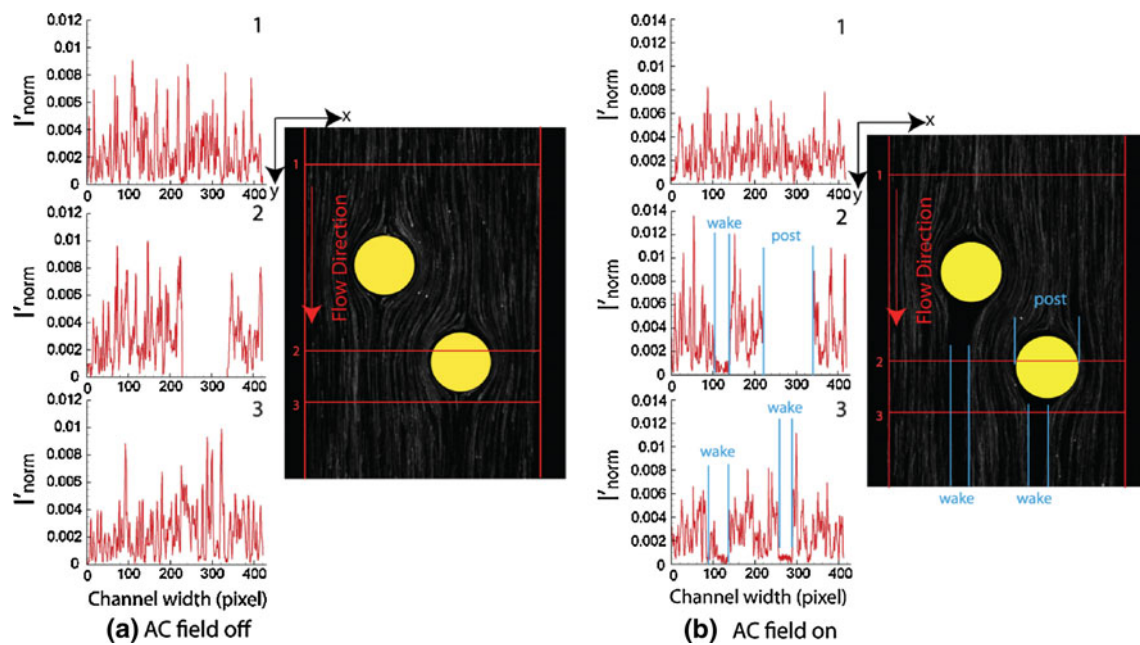


Fig. 6 Intensity profile of moving particles at three cross-sections in a microfluidic device with two posts and pressure-driven background flow: **a** AC field is off, **b** AC field is on, $V = 50$ Vp-p

near-field region and the far-field region. These devoid regions are dark, continuing out of the image in the downstream direction. The width of these regions depends on the strength of the applied field (Fig. 7). The width of the wake region at a location $100\ \mu\text{m}$ downstream of the posts is approximately 23 and $36\ \mu\text{m}$ for applied voltage of 35 Vp-p and 50 Vp-p, respectively (numerical models support the prediction of increased effects at increased applied voltage, presuming no reactions are happening at the surface).

As expected, for low frequencies (e.g. 5 Hz), DC effects are present but they become suppressed when the frequency is increased to approximately 50 Hz. This limit is derived from experimental observations of the DC motion of suspended particles which cease reacting to the AC field at frequencies above 30 Hz. At frequencies above this level, the fluid and particles in the channel do not have time to reach steady state velocities; such behavior is observed at a frequency where the particles stop vibrating and revert to random thermal motion. This establishes a set of bounds on the frequency of the applied AC electric field to be used in both the numerical and experimental investigations of a minimum of 50 and a maximum of 300 (refer to Sect. 2 for discussion). It has been theorized (Storey et al. 2008) and observed (Harnett et al. 2008) that ICEO velocities decrease as the AC frequency is increased due to an increase in viscosity in the EDLs from a large concentration of ions. Therefore, the numerical and experimental tests were conducted with an AC frequency of 50 Hz. No difference in the pattern of the regions devoid of particles was observed when the frequency was changed over the range of 50 – 300 Hz.

With the AC field on, the intensity profiles show a random distribution of particles at position one (upstream of the posts), whereas at positions two and three (downstream of the posts), the particle distribution is suppressed at one and two spanwise locations in the wake, respectively (Figs. 5b, 6b). Note that the obvious lack of particle counts across the post at position two is simply a representation of the post location.

These regions devoid of particles demonstrate a slight focusing effect on the flow of particles between the post and the walls (Fig. 5b) and also between the posts (Fig. 6b). Three horizontal lines in Figs. 5 and 6 indicate the location of the cross-sections across which the presence of particles was quantified. Creation of multiple streams can be achieved by using more than one post in the channel (Figs. 6b, 7b, c). Other forms of flow focusing, often manifested as the creation of particle streams, have often been proposed for sensing and detection applications (e.g. Mao et al. 2007); multiple streams may offer the potential for multiplexed detection schemes. In the present case, particles that pass between the posts occupy a slightly smaller spanwise region because of the wakes. In order to be used in practical applications, the focusing effect should be increased. One potential option is to increase the strength of the electric field or size of the posts. The present experiments indicate that the possibility of flow focusing or the creation of multiple particle/particle-free streams are real and a potentially important application for ICEO flows.

A direct comparison of the numerical models to the experimental case is provided in Fig. 8b. The numerical

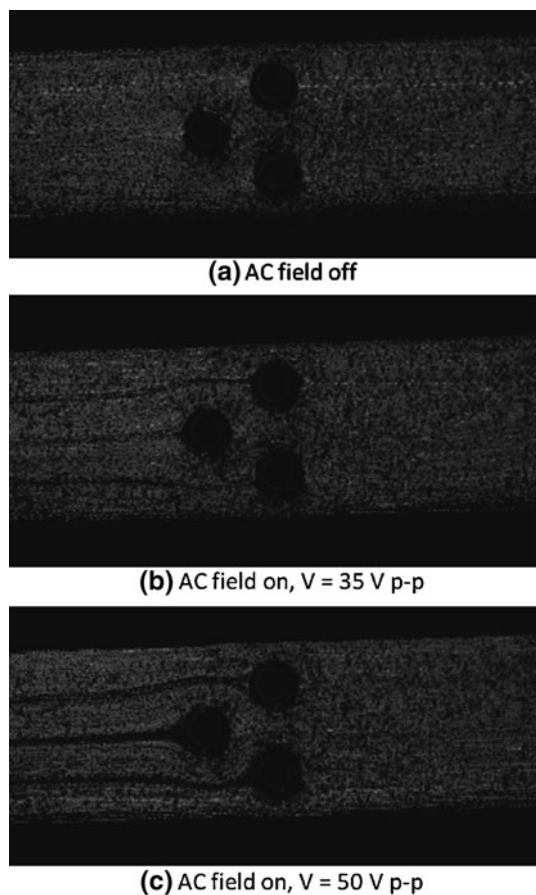


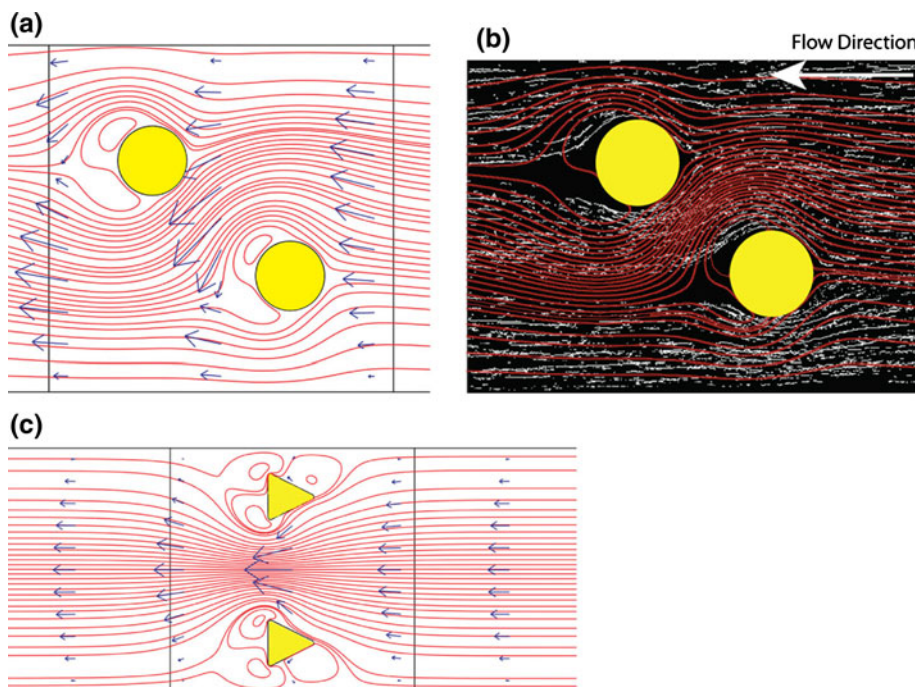
Fig. 7 Multiple regions devoid of particles downstream of three conductive posts: **a** Flow is driven by pressure difference and AC field is off, **b** AC field applied at field frequency of 50 Hz and voltage of 35 Vp-p, **c** AC field applied at field frequency of 50 Hz and voltage of 50 Vp-p

fluid streamlines predict the presence of recirculation regions on the downstream side of the particle, while the upstream recirculation regions are absent. The present numerical models are matched as precisely as possible to the experimental results in Fig. 8b by matching the physical parameters of the system (dimensions, physical characteristics of fluid, etc.), where the numerical streamlines are superimposed on the experimental image.

A few points of interest deserve discussion at this point. First, polystyrene (PSL) particles typically have a negative surface charge, leading to the question as to whether or not the surface charge is wholly responsible for the flow modification in the post region. Also, results from only one size (1 μm) of PSL tracer particles are shown herein. On both accounts, alternative tracers were used in microchannels with similar geometries (fabricated in the same batch). These alternatives were smaller particles (500 nm) and dye, both of which have different physical characteristics from the 1-μm particles. In both cases, the qualitative flow structure appears to be the same given the same channel and obstacle geometries. Quantitative comparisons are not possible due to (i) the impossibility of reusing the same exact channel due to fouling during an experimental run, and (ii) constraints of the flow measurement system and low signal-to-noise ratio on digital recordings. However, the preliminary visualizations suggest that surface charge of the particle cannot be solely responsible for the changes in flow structure under applied AC field.

Additionally, any recirculation regions “behind” (downstream) of the post are difficult to see using this visualization method. Given the physical constraint of

Fig. 8 Comparison of the numerical models to the experimental results. **a** Fluid streamlines with a pressure difference providing the background flow, **b** fluid streamlines from the numerical model in **b** overlaid on the experimentally observed streamlines, **c** example of a potential flow-focusing device proposed for the next generation of ICEO devices



magnification, and thus level of signal, the primary method of “viewing” the flowfield was by building up streamlines over a series of frames. While visually (by eye) some evidence of recirculation has been observed, it is suggested that the limited number of particles in the recirculation region simply do not provide enough signal-to-noise ratio in our experiments for definitive digital viewing. At least three explanations for the wakes can be hypothesized, namely: that they are an artifact of visualization (as may be the case in Harnett et al. 2008, Fig. 2a); that they are an effect of particle surface charge despite the precedent set by both Harnett et al. (2008) and Levitan et al. (2005) for using them as tracer particles and our experience qualitatively observing similar flow behavior using simply dye; or that the inertia of the particle is coming into play (again refuted somewhat by the qualitative similarity when using dye visualization).

The lithographically-based manufacturing method employed here enables the opportunity to explore additional geometries of the conducting posts to further tailor the device to the desired application. The use of cylindrical posts creates symmetrical ICEO flow in the absence of background flow. Use of conducting posts that are also no longer symmetric, with respect to the applied AC electric field, is expected to produce ICEO flow patterns that are no longer symmetric and can be tailored so that the ICEO flow is favorable to the desired flow manipulation. An example is the use of triangular conducting posts with one vertex aligned into the oncoming background flow, such as the posts in Fig. 8c. The magnitude of the ICEO flow around the triangular posts, oriented as such, is greater on the downstream side of the post. These expected patterns could lead to an increased focusing effect compared to the circular posts used earlier.

6 Conclusions

ICEO flows near conducting structures provide an on/off switchable means of manipulating fluid flow and particles suspended therein in a microfluidic device. The applications to lab-on-a-chip technologies are many, including manipulation of suspended biological materials, the creation of materials, or fabrication. A novel fabrication technique was used to create various designs of conducting posts with different sizes, shapes, numbers, and locations. Furthermore, the method contains the flexibility and precision to enable a wide range of design possibilities. ICEO flows are driven by the application of an AC electric field and so can provide intermittent focusing or single/multiple streaming effects or a varied strength of effect by cycling the field or altering its magnitude. This streaming as a function of applied AC field has not previously been

demonstrated experimentally. The successful observations of such phenomena demonstrate the promising nature of ICEO for particle manipulation.

Acknowledgments The authors acknowledge support from The Pennsylvania State University Materials Research Institute Nano Fabrication Network and the National Science Foundation Cooperative Agreement No. 0335765, National Nanotechnology Infrastructure Network, with Cornell University. This material is also based upon the work supported by the National Science Foundation under Grant No. 0348149. We appreciate the assistance provided by the PSU High Performance Computing Group, Guy Lavallee, Jinjie Shi, and Dr. Michael L. Jonson.

References

- Ajdari A (2000) Pumping liquids using asymmetric electrode arrays. *Phys Rev E* 61:45–48
- Appleyard DC, Lang MJ (2007) Active particle control through silicon using conventional optical trapping techniques. *Lab Chip* 7:1837–1840
- Bazant M, Thornton K, Ajdari A (2004) Diffuse-charge dynamics in electrochemical systems. *Phys Rev E* 70:1–24
- Bazant MZ, Kilic MS, Storey BD, Ajdari A (2009a) Nonlinear electrokinetics at large voltages. *New J Phys* 11:1–9
- Bazant MZ, Kilic MS, Storey BD, Ajdari A (2009b) Towards an understanding of induced-charge electrokinetics at large applied voltages in concentrated solutions. *Adv Colloid Interface Sci* 152:1–69
- Chiou PY, Ohta AT, Wu MC (2005) Massively parallel manipulation of single cells and microparticles using optical images. *Nature* 436:370–372
- Cong H, Hong L, Harake RS, Pan T (2010) CNT-based photopatternable nanocomposites with high electrical conductivity and optical transparency. *J Micromech Microeng* 20:1–6
- Daghighi Y, Li D (2010) Induced-charge electrokinetic phenomena. *Microfluid Nanofluid*. doi:10.1007/s10404-010-0607-2
- Davison SM (2009) Experimental and numerical analysis of the electrophoretic control of nanowires. Dissertation, The Pennsylvania State University
- Demierre N, Braschler T, Linderholm P, Seger U, Van Lintel H, Renaud P (2007) Characterization and optimization of liquid electrodes for lateral dielectrophoresis. *Lab Chip* 7:355–365
- Desai JP, Pillarisetti A, Brooks AD (2007) Engineering approaches to biomanipulation. *Ann Rev Biomed Eng* 9:35–53
- Dinsmore AD, Yodh AG, Pine DJ (1996) Entropic control of particle motion using passive surface microstructure. *Nature* 383:239–242
- Eckstein Y, Yossifon G, Seifert A, Miloh T (2009) Nonlinear electrokinetic phenomena around nearly insulated sharp tips in microflows. *J Colloid Interface Sci* 338:243–249
- Gamayunov NI, Murtsovkin VA, Dukhin AS (1986) Pair interaction of particles in electric field. Part 1: features of hydrodynamic interaction of polarized particles. *Colloid J USSR* 48:197–203
- Harnett CK, Templeton J, Dunphy-Guzman KA, Senousy YM, Kanouff MP (2008) Model based design of a microfluidic mixer driven by induced charge electroosmosis. *Lab Chip* 8:565–572
- Hsu CH, Di Carlo D, Chen C, Irimia D, Toner M (2008) Microvortex for focusing, guiding and sorting of particles. *Lab Chip* 8: 2128–2134
- Hung Lh, Lee AP (2007) Microfluidic devices for the synthesis of nanoparticles and biomaterials. *J Med Biol Eng* 27:1–6
- Jain M, Yeung A, Nandakumar K (2009) Efficient micromixing using induced-charge electroosmosis. *J Microelectromech Syst* 18: 376–384

- Komen J, Wolbers F, Franke H, Andersson H, Vermes I, Van Den Berg A (2008) Viability analysis and apoptosis induction of breast cancer cells in a microfluidic device: effect of cytostatic drugs. *Biomed Microdevices* 10:727–737
- Levitan JA, Devasenathipathy S, Studer V, Ben Y, Thorsen T, Squires TM, Bazant MZ (2005) Experimental observation of induced-charge electro-osmosis around a metal wire in a microchannel. *Colloids Surf A* 267:122–132
- Liu RH, Lodes MJ, Nguyen T, Siuda T, Slota M, Fuji HS, McShea A (2006) Validation of a fully integrated microfluidic array device for influenza A subtype identification and sequencing. *Anal Chem* 78:4184–4193
- Liu D, Wang L, Zhong R, Li B, Ye N, Liu X, Lin B (2007) Parallel microfluidic networks for studying cellular response to chemical modulation. *J Biotechnol* 131:286–292
- Mao X, Waldeisen JR, Huang TJ (2007) Microfluidic drifting—implementing three-dimensional hydrodynamic focusing with a single-layer planar microfluidic device. *Lab Chip* 7:1260–1262
- Murtsovkin VA (1996) Nonlinear flows near polarized disperse particles. *J Colloid* 58:341–349
- Novak L, Neuzil P, Pipper J, Zhang Y, Lee S (2007) An integrated fluorescence detection system for lab-on-a-chip applications. *Lab Chip* 7:27–29
- Pascall AJ, Squires TM (2010) Induced charge electro-osmosis over controllably contaminated electrodes. *Phys Rev Lett* 104:1–4
- Ramos A, Morgan H, Green NG, Castellanos A (1998) AC electrokinetics: a review of forces in microelectrode structures. *J Phys D Appl Phys* 31:2338–2353
- Ramos A, Morgan H, Green N, Castellanos A (1999) The role of electrohydrodynamic forces in the dielectrophoretic manipulation and separation of particles. *J Colloid Interface Sci* 217:420–422
- Shi J, Mao X, Ahmed D, Colletti A, Huang TJ (2008) Focusing microparticles in a microfluidic channel with standing surface acoustic waves (SSAW). *Lab Chip* 8:221–223
- Soni G, Squires T, Meinhart C (2007) Nonlinear phenomena in induced charge electroosmosis. In: IMECE2007-41468 proceedings of 2007 ASME international mechanical engineering congress and exposition, Seattle, Washington
- Špringer T, Piliarik M, Homola J (2010) Surface plasmon resonance sensor with dispersionless microfluidics for direct detection of nucleic acids at the low femtomole level. *Sens Actuators B Chem* 145:588–591
- Squires TM, Bazant MZ (2004) Induced-charge electro-osmosis. *J Fluid Mech* 509:217–252
- Squires TM, Bazant MZ (2006) Breaking symmetries in induced-charge electro-osmosis and electrophoresis. *J Fluid Mech* 560:65–101
- Squires TM, Quake SR (2005) Microfluidics: fluid physics at the nanoliter scale. *Rev Mod Phys* 77:977–1026
- Storey BD, Edwards LR, Kilic MS, Bazant MZ (2008) Steric effects on AC electro-osmosis in dilute electrolytes. *Phys Rev E* 77(3):036317-1–036317-11
- Sugioka H (2010) Chaotic mixer using electro-osmosis at finite Péclet number. *Phys Rev E* 81:1–9
- Whitesides GM (2006) The origins and the future of microfluidics. *Nature* 442:368–373
- Zhang C, Khoshmanesh K, Mitchell A, Kalantar-Zadeh K (2010) Dielectrophoresis for manipulation of micro/nano particles in microfluidic systems. *Anal Bioanal Chem* 396:401–420
- Zhao C, Yang C (2009) Analysis of induced-charge electro-osmotic flow in a microchannel embedded with polarizable dielectric blocks. *Phys Rev E* 80:1–11